Network approach to the pinning control of drift-wave turbulence

Panpan Liu,[1,2] Zhigang Deng,[1,2] Lei Yang,[1] Meng Zhan,[3] and Xingang Wang[1,2,*]
[1]*Department of Physics, Zhejiang University, Hangzhou 310027, China*
[2]*School of Physics and Information Technology, Shaanxi Normal University, Xi'an 710062, China*
[3]*Wuhan Institute of Physics and Mathematics, Chinese Academy of Sciences, Wuhan 430071, China*
(Received 4 March 2014; published 18 June 2014)

Network of coupled oscillators has long been employed as an important approach to explore the complicated dynamics in spatially extended systems. Here we show how this approach can be used to the analysis of turbulence pinning control. Specifically, by use of a model of two-dimensional drift-wave plasma turbulence, we investigate how the performance of the turbulence control is influenced by the spatial distribution of the pinning strength. It is found that the dynamics of pinned turbulence can be well captured by a simple model of networked modes, based on which the dependence of the control performance on the pinning distribution can be analytically obtained. In particular, the model predicts that as the distribution of the pinning strength becomes more nonuniform, the performance of turbulence control will be gradually decreased. This theoretical prediction is in good agreement with the results of numerical simulations, including the sinusoidal and localized pinning distributions. Our studies provide a new viewpoint to the mechanism of mode couplings in drift-wave turbulence, as well as be constructive to the design of new schemes for controlling turbulence in realistic systems.

DOI: 10.1103/PhysRevE.89.062918 PACS number(s): 05.45.Gg, 05.45.Xt

I. INTRODUCTION

Chaos control has been a central topic in nonlinear science for decades [1,2]. Since the pioneer work of Ott, Grebogi, and York in 1990 [3], tremendous efforts had been given to the control of chaos in various circumstances, in which a variety of controlling techniques had been developed [4,5]. While the earlier studies are more concerning with the control of low-dimensional chaos, recently much more attentions have been given to the control of spatiotemporal chaos [6–8], motivated by the omnipresent existence of spatially extended dynamical systems in nature. Differing from low-dimensional chaos, in spatiotemporal chaos the unstable manifold is generally of very high dimension, as characterized by the existence of a large number of positive Lyapunov exponents [2]. This feature makes many techniques developed for controlling low-dimensional chaos no more applicable, thus leading to the search of new approaches for controlling spatially extended systems [8–10]. Among the new approaches proposed in the literature, pinning control is distinguished from others by its efficiency, flexibility, and high performance and has been widely adopted for controlling spatiotemporal chaos in various systems, including ensembles of chaotic oscillators on an array or lattices [11–13], spatiotemporal chaos described by partial differential equations [14–17], defect turbulence in cardiac systems [18], and flow turbulence described by the Novier-Stokes equations [19–21].

A typical example of spatiotemporal nonlinear system that has been extensively studied in literature is the drift-wave turbulence, which arises naturally in magnetic plasmas where pressure gradient exists [22]. Drift-wave turbulence is generally believed to be responsible for the anomalous cross-field particle transport [23], and its control and suppression therefore is of great importance to the performance of magnetic confinement fusion devices, e.g., the tokamaks [24]. Over the past two decades, there have been continuous attempts in extending the techniques developed in chaos control to the suppression of drift-wave turbulence, in which a variety of theories and techniques have been proposed [25–32]. In the regime of weak turbulence, by use of the technique of time-delay autosynchronization (TDAS) [33], it has been shown by a series of studies that the chaotic temporal behavior of the drift waves in cylindrical magnetized plasmas can be tamed to be periodic [25,27,31]. Moreover, by the strategy of open-loop synchronization, namely the mode-selective control, it has been shown recently that the complicated spatial behavior of the weakly developed drift-wave turbulence can be also successfully controlled (synchronized) to a predefined pattern of regular spatial structure [29,30]. More recently, by use of the method of pinning coupling, it has been shown that both the spatial and temporal behaviors of the drift-wave turbulence can be efficiently regulated into different spatiotemporal patterns, given the pinning strength is larger to some critical value [34].

As in chaos control, the control of drift-wave turbulence relies also on a proper understanding of the system dynamics [27,29,34]. This is reflected not only in the selection of the targeting states but also in the design of the control signals, i.e., the controlling strategy. In exploring the dynamics of drift-wave turbulence, a general approach is to transform the problem into the Fourier space, and investigating how the interactions of the modes, i.e., the mode-mode couplings, lead to complicated system behaviors. Along this approach, several classic models have been proposed in the literature [35–37], which well explains the transition from regular to chaotic behaviors, as well as the self-organization of some large-scale structures, e.g., the zonal flows [38]. However, these models describe only the situation of free turbulence (autonomous system) and are not suitable for analyzing the turbulence control. In turbulence control, the key idea is to establish an efficient coupling between the targeting state and some intrinsic wave modes in the system to enhance these specific modes while suppressing the others [19–21]. This feature makes it necessary to include the targeting state as a

*Corresponding author: wangxg@snnu.edu.cn

part of the system when analyzing the mode couplings. This is specially the case when the controlling signals satisfy certain spatial distribution, in such a case the mode couplings might significantly modified due to the new resonance induced by the controlling signals. That is, to analyze the turbulence control, the current models of mode couplings should be improved.

The purpose of the present work is to investigate the control of drift-wave turbulence under distributed pinning, based on a network model of coupled modes. Here, distributed pinning refers to the situation that the strength of the pinning coupling is varying in the space and satisfies certain distributions, e.g., the sinusoidal form or localized distribution [11,12]. This is an important extension of the strategy of global pinning studied in Ref. [34], in which the pinning couplings are added on each site of the system with a constant strength. Comparing to the case of global pinning, distributed pinning is more convenient and practicable in operation, as in realistic situations the state of the whole system is generally not available. It worth noting that while the feasibility of distributed pinning has been well verified in controlling spatiotemporal chaos (or weak turbulence), it is still not clear whether it can be applied to fully developed turbulence, e.g., the strong drift-wave turbulence [19,20]. Motivated by these, we in the present work investigate the control of fully developed drift-wave turbulence by distributed pinning, with special attention being paid to the influence of the pinning distribution on the the control performance. Our main finding is that, with the increase of the pinning nonuniformity (which in sinusoidal pinning distribution is characterized by the decreased wave number or increased amplitude), it becomes more difficult to control the turbulence. We demonstrate this finding by extensive numerical simulations and analyze its underlying mechanisms by theoretical analysis based on a new model of networked modes.

The rest of the paper is organized as follows. In Sec. II, by numerical simulations, we shall demonstrate the control of drift-wave turbulence by sinusoidal pinning and study the influence of the pinning distribution on the turbulence control performance. In Sec. II, we shall analyze the system dynamics in the Fourier space and propose the new model of networked modes. The dynamics of the network model is analyzed in detail in Sec. III, in which an explicit formula is obtained on the influence of the pinning distribution on control performance. In Sec. IV, we shall extend our studies to the case of localized control and give the conclusion.

II. NUMERICAL RESULTS

The drift-wave plasma turbulence to be investigated is described by the following two-dimensional (2D) Hasegawa-Mima equation [39]:

$$\partial_t(1-\nabla_\perp^2)\phi + V_d\partial_y\phi + [\nabla_\perp^2\phi,\phi] = 0, \qquad (1)$$

with $\phi = \phi(x,y,t)$ as the electrostatic potential, $[f,g] = \partial_y f\partial_x g - \partial_x f\partial_y g$ as the Poisson bracket, and $\nabla_\perp^2 = \nabla_x^2 + \nabla_y^2$ as the Laplace operator perpendicular to the magnetic field $\mathbf{B} = B\mathbf{e}_z$. Standard operations have been adopted to make the equation dimensionless, and the only tunable parameter of the equation is V_d, which characterizes the speed of the diamagnetic drift. The nonlinearity of the equation lies in the term $[\nabla_\perp^2\phi,\phi]$, which is caused by the nonlinear polarization drift. Throughout the study, we will fix $V_d = 1$, with which the system is in the strong turbulence regime [40].

In numerical simulations, we set the system to be bounded in the square domain $[0,8\pi] \times [0,8\pi]$ and adopt the periodic boundary condition for each direction. The time increment Δt is chosen as 1×10^{-2} [in obtaining Eq. (1), the time t has been normalized by the ion gyroperiod], and the space is divided into 128×128 grids. The initial conditions are given in the Fourier space, which, for the sake of simplicity, are chosen as a combination of three plane waves, $\phi(t=0) = \sum_{i=1}^{3} A_0 \cos(\mathbf{k}_i \cdot \mathbf{r})$, with $A_0 = 1 \times 10^{-2}$ and $\mathbf{k}_1 = (1,2), \mathbf{k}_2 = (1,3), \mathbf{k}_3 = (-3,-5)$. To integrate the equation, we adopt the Fourier pseudospectral method and the Adams-Bashforth-Crank-Nicolson (ABCN) scheme for the space and time discretizations, respectively [34,41]. The numerical results are verified by using different initial conditions, grids, and time increments. The equation is integrated for a period of length $t = 1 \times 10^3$, during which the system shows the typical behavior of 2D drift-wave turbulence, e.g., the formation, interaction, and evolution of vortices. The distribution of ϕ at the moment $t = 1 \times 10^3$ is presented in Fig. 1(a), which shall be taken as the reference turbulence to be controlled by distributed couplings in our studies.

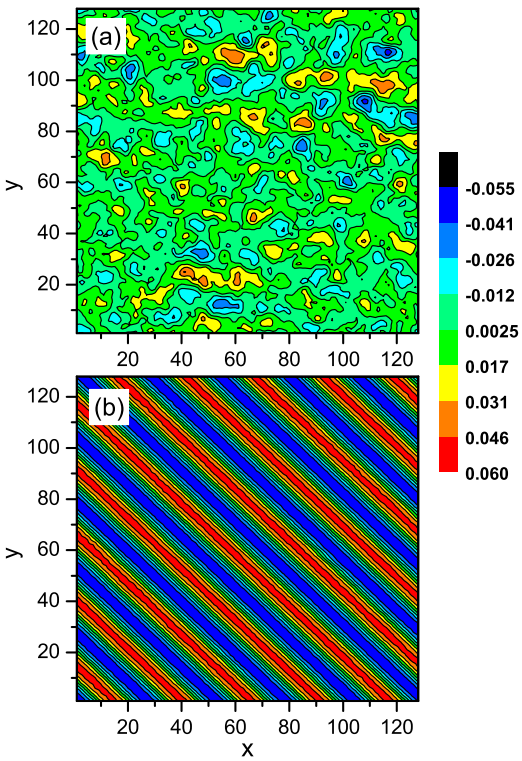

FIG. 1. (Color online) (a) The equipotential contours of ϕ for the 2D drift-wave turbulence described by the Hasegawa-Mima equation. (b) By the sinusoidal pinning of parameters $\varepsilon_0 = 0.12$, $A^p = 1.0$, and $k^p = 0.75$, the contours of ϕ at the moment $t = 1 \times 10^3$ after the start of the pinning control. It is seen that the turbulence in (a) is well controlled to the target pattern $\phi_T = A_T \cos(\mathbf{k}_T \cdot r - \omega_T t)$, with $A_T = 5 \times 10^{-2}$ and $k_T = 1.25$.

When distributed pinning is added, the equation of the system dynamics reads

$$\partial_t(1-\nabla_\perp^2)\phi + V_d\partial_y\phi + [\nabla_\perp^2\phi,\phi] = \varepsilon(x,y)(\phi-\phi_T). \quad (2)$$

Here ϕ_T is the spatiotemporal pattern that the turbulence is going to be controlled to, i.e., the target. In the present work, we choose the target as one of the unstable solutions of the Hasegawa-Mima equation, $\phi_T = A_T\cos(\mathbf{k}_T\cdot\mathbf{r}-\omega_T t)$, with $\mathbf{k}_T = (k_T,k_T)$ and $\omega_T = k_T/(1+k_T^2)$. Differing from previous studies, in Eq. (2) the pinning strength ε is varying in the space, $\varepsilon(x,y) = \varepsilon_0[1+\phi^p(x,y)]$, with ε_0 the uniform pinning strength and ϕ^p the pinning function. In our first study, we set ϕ^p to satisfy the sinusoidal form, i.e., $\varepsilon(x,y) = \varepsilon_0[1+A^p\cos(k_x^p x + k_y^p y)]$. A^p reflects the degree of variation for the pinning strength and is named the pinning amplitude. $\boldsymbol{k}^p$ characterizes the distribution of the pinning strength over the space and is named the pinning wave number. For the sake of simplicity, we set $k_x^p = k_y^p = k^p$. Apparently, by increasing A^p or decreasing k^p, the distribution of the pinning strength will be gradually changed from uniform to nonuniform. Our main task in the present work is just to investigate how the change of A^p and $k_{x,y}^p$ will affect the control performance for the drift-wave turbulence. (Please note that by changing A^p and k^p, the total pinning cost is kept unchanged, i.e., $\sum\varepsilon(x,y) = \text{const}$. For this reason, the question we are interested here could be also regarded as a problem of pinning optimization.)

We start by checking the controllability of the drift-wave turbulence by distributed pinning. Differing from spatiotemporal chaos, where distributed pinning has been justified and effective, it remains an open question whether strong turbulence is controllable by distributed pinning [20]. Setting $A_T = 5\times10^{-2}$ and $k_T = 1.25$ for the target (which will be fixed throughout the following studies), and using $\varepsilon_0 = 0.12$, $A^p = 1.0$, and $k^p = 0.75$ for the pinning distribution, we plot in Fig. 1(b) the contours of ϕ at $t = 1\times10^3$ after the start of the pinning control. It is seen that the turbulence shown in Fig. 1(a) is successfully controlled to the target $\phi_T = A_T\cos(\mathbf{k}_T\cdot\mathbf{r}-\omega_T t)$.

Having justified the efficiency of distributed pinning on controlling drift-wave turbulence, we go on to study the dependence of the control performance on the pinning parameters. The performance of pinning control is evaluated by the normalized control error, $\sigma = \sqrt{\sum_{i,j}^N(\phi_{i,j}-\phi_T)^2/N^2}/A_T$, with $N = 128$ the size of the simulation grid. In simulation, σ is calculated at the moment $t = 1\times10^3$ after the start of the pinning control. Clearly, the smaller is σ, the better is the system controlled to the target. To study, we change the pinning wave number k^p and pinning amplitude A^p in the sinusoidal distribution and check how the value of σ is varied.

The dependence of σ on k^p is shown in Figs. 2(a) and 2(b). In Fig. 2(a), we fix the pinning amplitude $A^p = 1.0$ and plot σ as a function of ε_0 for different values of k^p. It is seen that, for the given k^p, σ is gradually decreased with the increase of ε_0. Also, in Fig. 2(a), it is seen that the control performance is affected by the pinning wave number. More specifically, with the decrease of k^p, the value of σ is found to be increased. To have more details on the dependence of σ on k^p, we fix $\varepsilon_0 = 0.15$, and plot in Fig. 2(b) the variation of

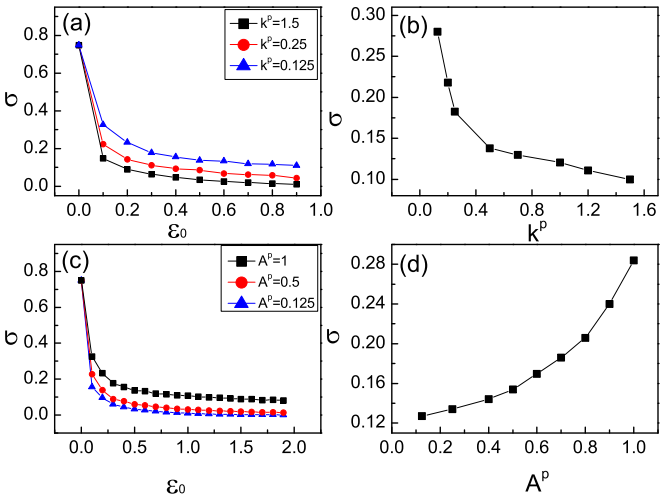

FIG. 2. (Color online) Numerical results on the influence of the pinning distribution on the control performance. (a) Fixing $A^p = 1.0$, the variation of the normalized pinning error σ as a function of the uniform pinning strength ε_0 for different pinning wave numbers k^p. (b) Fixing $\varepsilon_0 = 0.15$ in (a), the variation of σ as a function of k^p. (c) Fixing $k^p = 0.125$, the variation of σ as a function of ε_0 for different pinning amplitudes A^p. (d) Fixing $\varepsilon_0 = 0.15$ in (c), the variation of σ as a function of A^p.

σ as a function of k^p. Now it is seen that with the increase of k^p, σ is monotonically decreased.

The influence of A^p on σ is presented in Figs. 2(c) and 2(d). Fixing the pinning wave number $k^p = 0.125$, we plot in Fig. 2(c) the variation of σ as a function of ε_0 for different values of A^p. It is observed that with the increase of A^p, the curve of control error seems to be shifting upwards. This trend is confirmed in Fig. 2(d), in which we fix $\varepsilon_0 = 0.15$ and plot σ as a function of A^p. It is clearly seen that with the increase of A^p, the control error is increased in a monotonic fashion. The numerical results of Fig. 2 thus suggest that *by increasing the pinning amplitude A^p or decreasing the pinning wave number k^p, the turbulence becomes more difficult to be controlled.* Our mission in the following sections is to explain these numerical phenomena, based on a new model of networked modes.

III. NETWORK MODEL

To explore the dynamics of the pinned turbulence, we transform Eq. (2) into the Fourier space, and investigate how the drift waves (modes) are interacting with each other. Rewriting $\phi = \sum_i[\hat{\phi}_i(t)\exp(i\mathbf{k}_i\cdot\mathbf{r})+c.c]/2$, $\phi_T = [\hat{\phi}_T(t)\exp(i\mathbf{k_T}\cdot\mathbf{r})+c.c]/2$, and $\phi^p = [A^p\exp(i\mathbf{k}^p\cdot\mathbf{r})+c.c]/2$, Eq. (2) then is changed to

$$\begin{aligned}\sum_i(\partial_t + i\omega_i' + \varepsilon_i')\hat{\phi}_i(t)e^{i\mathbf{k}_i\cdot\mathbf{r}} &= \sum_{l,j}\Lambda_{lj}^i\hat{\phi}_l^*(t)\hat{\phi}_j^*(t)^{-i(\mathbf{k}_l+\mathbf{k}_j)\cdot\mathbf{r}} \\ &+ \varepsilon_i'\hat{\phi}_T(t)e^{i\mathbf{k}_T\cdot\mathbf{r}} + \varepsilon_i'A^p\hat{\phi}_T^*(t)e^{-i(\mathbf{k}^p+\mathbf{k}_T)\cdot\mathbf{r}} \\ &- \varepsilon_i'\sum_m\hat{\phi}_m^*(t)A^p e^{-i(\mathbf{k}_m+\mathbf{k}^p)\cdot\mathbf{r}}, \end{aligned} \quad (3)$$

with $\omega_i' = V_d k_{iy}/(1+\mathbf{k}_i^2)$, $\varepsilon_i' = \varepsilon_0/(1+\mathbf{k}_i^2)$, and $\Lambda_{lj} = (\mathbf{k}_j^2 - \mathbf{k}_l^2)(\mathbf{k}_j\times\mathbf{k}_l)\cdot\mathbf{e}_z/[2(1+\mathbf{k}_l^2)]$. $\hat{\phi}_i(t) = A_i(t)\exp(-i\omega_i t)$ and

$\hat{\phi}_T(t) = A_T \exp(-i\omega_T t)$ are, respectively, the temporal part of the electrostatic mode ϕ_i and the target ϕ_T. Without pinning, we have $\varepsilon' = 0$, and only the first term on the right-hand-side of Eq. (3) exists, which describes the traditional scheme of three-wave coupling and is the underlying mechanism for generating turbulence. When uniform pinning is applied, i.e., $\varepsilon' > 0$ and $A^p = 0$, the secnd term on the right-hand side of Eq. (3) will be activated, which corresponds to the situation of global pinning. When distributed pinning is employed, the last two terms on the right-hand side of Eq. (3) will be participated in, which, as we will show later, is the key in understanding the performance of distributed pinning.

By Fourier transform, we can obtain from Eq. (3) an infinite set of coupled ordinary differential equations, with each equation defines the evolution of a specific mode. Depending on whether the mode is directly driven by the target, the mode equations can be roughly classified into two types. The first type of mode equations reads

$$(d/dt + i\omega_i' + \varepsilon_i')\hat{\phi}_i(t) = \sum_{l,j} \Lambda^i_{l,j} \hat{\phi}^*_l(t)\hat{\phi}^*_j(t) - \varepsilon_i' A^p \hat{\phi}_m(t), \tag{4}$$

where the summation is over all wave vectors satisfying the resonant condition $\mathbf{k}_i + \mathbf{k}_l + \mathbf{k}_j = 0$. The control signals are reflected in the second term on the right-hand side of Eq. (4), which shows that, by the resonant condition $\mathbf{k}_i + \mathbf{k}_m + \mathbf{k}^p = 0$, the mode $\hat{\phi}_i$ is coupled to another mode $\hat{\phi}_m$ with the coupling strength $\varepsilon_i' A^p$. By the technique of mode truncation, we keep only a pair of resonant modes in the summation, e.g., $\hat{\phi}_{j,l}$. As such, the equation is simplified to be involving only four modes, $\hat{\phi}_{i,j,l,m}$. The coupling structure of these modes can be schematically represented by a network motif, as plotted in Fig. 3(a). In this motif, each node represents a specific mode, and a link represents that the modes it connects are coupled through the resonant conditions. As Eq. (4) applies to the general modes, this motif structure is typical in the system, which is the first block constituting our network model.

The second type of mode equations applies to only two special modes. The first one, which is denoted as ϕ_c and named as the control mode here, has the same wave number and frequency as the target, i.e., $\phi_c = A_c(t)\exp(i\boldsymbol{k}_c \cdot \boldsymbol{r} - i\omega_c t) = A_c(t)\exp(i\boldsymbol{k}_T \cdot \boldsymbol{r} - i\omega_T t)$. The evolution of $\hat{\phi}_c(t) = A_c(t)\exp(-i\omega_T t)$ is governed by the equation

$$\begin{aligned}(d/dt + i\omega_c' + \varepsilon_c')\hat{\phi}_c(t) =& \sum_{l,j} \Lambda^c_{l,j} \hat{\phi}^*_l(t)\hat{\phi}^*_j(t) \\ &- \varepsilon_c' A^p \hat{\phi}^*_m(t) + \varepsilon_c' \hat{\phi}_T(t).\end{aligned} \tag{5}$$

As $\boldsymbol{k}_c = \boldsymbol{k}_T$, we have $\varepsilon_c' = \varepsilon_T'$ and $\omega_c' = \omega_T'$. Comparing to Eq. (4), a new term, $\varepsilon_c'\hat{\phi}_T(t)$, appears on the right-hand side of Eq. (5), which represents the driving received from the target. As $A^p < 1$ and $\hat{\phi}_m < \hat{\phi}_T$ (i.e., the intrinsic modes are always weaker than the target), $\hat{\phi}_c$ is more influenced by $\hat{\phi}_T$ than $\hat{\phi}_m$. This makes it reasonable to neglect the influence of $\hat{\phi}_m$ in Eq. (5). Considering again only a pair of resonant modes in the summation, $\hat{\phi}_{l,j}$, and replacing ε_c' with ε_T' and ω_c' with ω_T', Eq. (5) then is simplified to

$$(d/dt + i\omega_T' + \varepsilon_T')\hat{\phi}_c(t) = \Lambda^T_{l,j}\hat{\phi}^*_l(t)\hat{\phi}^*_j(t) + \varepsilon_T'\hat{\phi}_T(t), \tag{6}$$

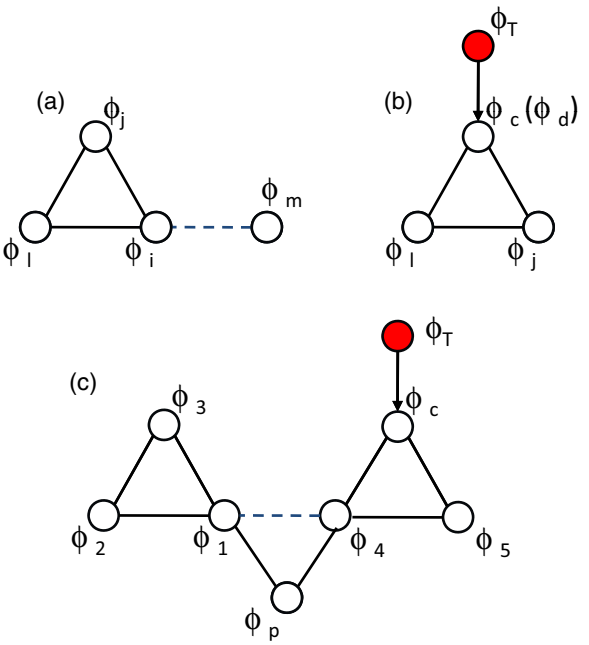

FIG. 3. (Color online) Schematic plots on the structure of mode couplings when distributed pinning is added to the drift-wave turbulence. (a) For the typical mode ϕ_i described by Eq. (4), its couplings to other three modes ϕ_l, ϕ_j, and ϕ_m. The dashed line denotes that the coupling strength between ϕ_i and ϕ_m is also dependent on the pinning amplitude A^p. (b) For the special mode ϕ_c (ϕ_d) described by Eq. (6) [Eq. (7)], its couplings to other two modes ϕ_l and ϕ_j, as well as its coupling to the target ϕ_T. The arrowed line represents the unidirectional coupling from the target. (c) The network model that combines (a) and (b), which is used in the present work to investigate the control performance of distributed pinning.

Still, the coupling structure of the modes can be schematically represented by a network motif, which is shown in Fig. 3(b). It worth noting that in Fig. 3(b) the target, ϕ_T, is coupled to the control mode, ϕ_c, in the one-way fashion (which is the nature of pinning control), while the other modes are coupled mutually.

The other special mode of the second type, ϕ_d, satisfies the resonant condition $\boldsymbol{k}^p + \boldsymbol{k}_T + \boldsymbol{k}_d = 0$, which is obtained by keeping the first, third, and fourth terms on the right-hand side of Eq. (3). By the similar approximation used in obtaining Eq. (6), we can obtain the evolution equation for this special mode,

$$(d/dt + i\omega_d' + \varepsilon_d')\hat{\phi}_d(t) = \Lambda^d_{l,j}\hat{\phi}^*_l(t)\hat{\phi}^*_j(t) + \varepsilon_d' A^p \hat{\phi}^*_T(t). \tag{7}$$

Equation (7) is essentially the same as Eq. (6), except the coupling strength $\varepsilon_d' A^p$ received from the target. As such, the couplings of the modes in Eq. (7) can be still represented by the network motif shown in Fig. 3(b) by simply replacing ϕ_c with ϕ_d.

Our above analysis of mode couplings implies that in the Fourier space the system dynamics is essentially captured by a complex network [42], in which nodes are the drift-wave modes and links are the couplings established by various resonant conditions. This network is constituted by numerous network motifs plotted in Fig. 3(a), together with two special

network motifs plotted in Fig. 3(b). The pinning signals, which are added onto each site in the original spatial space, now are added onto only two special modes in the network, ϕ_c and ϕ_d. As such, the problem of turbulence control we are interested now becomes the pinning control of a complex network–a topic that has arisen many research interest in network science in recent years [43–45]. From the viewpoint of network science, the network dynamics is said to be successfully controlled if the control mode, ϕ_c, is excited to be with large amplitude, while all other modes in the network are suppressed to 0. This picture of complex network, however, is still too complicated for theoretically treatment. As the central task of pinning control is to excite the control mode ϕ_c, modes surrounding ϕ_c in the network thus is of focusing interest in investigating the control performance. For this reason, we adopt only skirts representative modes around ϕ_c in the network and construct the simplified network model shown in Fig. 3(c). This simplified model, which basically is a combination of the motifs shown in Figs. 3(a) and 3(b), captures the essence of the mode couplings and, as we will demonstrate later, is able to explain the numerical results on the performance of distributed pinning (Fig. 1).

To make the resonant conditions closed, we have also included the mode ϕ_p in the network model. This mode has the same wave number as the pinning distribution, i.e., $\boldsymbol{k}_p = \boldsymbol{k}^p$, but are coupled to other two modes, ϕ_1 and ϕ_4, in the system. Thus, together with the target, ϕ_T, the network model actually consists of eight nodes. Although the pinning signals are added onto only the control mode ϕ_c, it is hoping that by the mode couplings, the other modes in the network could be also successfully suppressed. That is, the mode ϕ_c is excited to be with large amplitude, while the amplitude of the other modes are damped to 0. It should be noted that the network links are of different weight, as the coupling strength of a link is dependent on the modes they are connecting. Say, for instance, the coupling strength between modes ϕ_1 and ϕ_4 in the model is dependent on not only the wave number $\boldsymbol{k}_p$ (through the resonant condition $\boldsymbol{k}_1 + \boldsymbol{k}_4 + \boldsymbol{k}^p = 0$) but also on the pinning amplitude A^p (through the resonant condition $\boldsymbol{k}_1 + \boldsymbol{k}_4 + \boldsymbol{k}^p = 0$). From the viewpoint of network science, nodes of large degree (the number of connections) play more important roles in determining the network dynamics [46,47]. It is thus expected that in our network model modes $\phi_{1,4}$ will differ in their behavior from that of others.

For the convenience of theoretical analysis, we restrict our study to the one-dimensional case, i.e., $\phi = \phi(x,t)$. In such a case, the set of mode equations describing the dynamics of the network model are specified to

$$
\begin{aligned}
d\hat{\phi}_c/dt &= \Theta_T\hat{\phi}_c + \Lambda^c_{4,5}\hat{\phi}^*_4\hat{\phi}^*_5 + \varepsilon'_T\hat{\phi}_T,\\
d\hat{\phi}_p/dt &= \Theta_p\hat{\phi}_p + \Lambda^p_{1,4}\hat{\phi}^*_1\hat{\phi}^*_4,\\
d\hat{\phi}_1/dt &= \Theta_1\hat{\phi}_1 + \Lambda^1_{2,3}\hat{\phi}^*_2\hat{\phi}^*_3 + \Lambda^1_{4,p}\hat{\phi}^*_4\hat{\phi}^*_p - \varepsilon'_1A^p\hat{\phi}^*_4\\
d\hat{\phi}_2/dt &= \Theta_2\hat{\phi}_2 + \Lambda^2_{1,3}\hat{\phi}^*_1\hat{\phi}^*_3,\\
d\hat{\phi}_3/dt &= \Theta_3\hat{\phi}_3 + \Lambda^3_{1,2}\hat{\phi}^*_1\hat{\phi}^*_2,\\
d\hat{\phi}_4/dt &= \Theta_4\hat{\phi}_4 + \Lambda^4_{c,5}\hat{\phi}^*_c\hat{\phi}^*_5 + \Lambda^4_{1,p}\hat{\phi}^*_1\hat{\phi}^*_p - \varepsilon'_4A^p\hat{\phi}^*_1\\
d\hat{\phi}_5/dt &= \Theta_5\hat{\phi}_5 + \Lambda^5_{c,4}\hat{\phi}^*_c\hat{\phi}^*_4,
\end{aligned}
\tag{8}
$$

with $\Theta = -(i\omega' + \varepsilon')$ and where ω', ε', and Λ are the same as in Eq. (3). Depending on the node degree (the number of coupled modes), the mode equations can be classified into three groups: the degree of modes $\phi_{p,2,3,5}$ is 2, the degree of mode ϕ_c is 3, and the degree of modes $\phi_{1,4}$ is 4. Following the network terminology, we name $\phi_{1,4}$ the hub mode and name modes $\phi_{p,2,3,5}$ the normal mode. Considering together the feature of weighted couplings, the model we have proposed thus can be classified as a weighted, heterogeneous network [42].

The equations of the hub nodes, $\phi_{1,4}$, desire special attentions. As shown in Eq. (8), these two modes are not only coupled to other normal modes in the network but also coupled mutually by the enhanced strength, $\Lambda\hat{\phi}^*_p - \varepsilon' A^p$. Unlike other couplings (where the strength is determined by only the wave numbers of the connected modes), the coupling strength between ϕ_1 and ϕ_4 is also dependent on the pinning amplitude, A^p. Specifically, by increasing A^p, only the coupling between ϕ_1 and ϕ_4 will be enhanced, while the other couplings are kept unchanged. It is also important to note that as the seven modes in the network are coupled through three resonant conditions, there are only four independent modes. Also, as $k_c = k_T$ and $k_p = k^p$, the number of independent modes is reduced to 2. Without loss of generality, in our following studies we choose ϕ_2 and ϕ_5 as the independent modes (the findings we are going to present is robust and is independent on the selection of the independent modes).

IV. MODEL ANALYSIS

Can the network model reproduce the phenomena obtained in numerical simulations, i.e., the increased (decreased) control error as a function of the pinning amplitude (pinning wave number) shown in Fig. 2? To investigate, we next give an analysis on the dynamics of the network model and check how the control performance is affected by the two pinning parameters: k^p and A^p. Using still the parameters $k_T = 1.25$ and $A_T = 5 \times 10^{-2}$ for the target, and setting $k_2 = 0.6$ and $k_5 = 2.8$ for the independent modes, in Fig. 4 we plot the variation of the normalized control error, σ', as a function of the pinning wave number, k^p, and the pinning amplitude, A^p. Here, the normalized control error is redefined as $\sigma' = [\sum_{i=1}^{5}(A_i^2(t) + A_p^2)/6]^{1/2}/A_T$, which counts for the averaged amplitude of the nonpinning modes in the network ($\hat{\phi}_{i,p} = A_{i,p}e^{-i\omega_{i,p}t}, i = i, \ldots, 5$). The initial conditions of the modes, $A_i(t=0)$, are randomly chosen within the range $(0, A_T)$, and the results are averaged over a period of $t \times 10^4$. It is seen in Fig. 4 that, with the increase of k^p (A^p), the value of σ' is decreased (increased) monotonically, with is consistent with the trends observed in direct numerical simulations (the results shown in Fig. 2).

To have more details on the dynamics of the pinned network, we go on to explore the time evolution of the individual modes. Fixing the pinning wave number as $k^p = 0.5$, we plot in Fig. 5 the time evolution of $A_{1,\ldots,5}$, A_c, and A_p. It is seen that during the process of network evolution, the control mode, A_c, is excited and stabilized to a large amplitude, while all other modes are finally damped to 0. That is, the network is successfully controlled to the target under the set of control parameters. Two interesting phenomena are also observed in

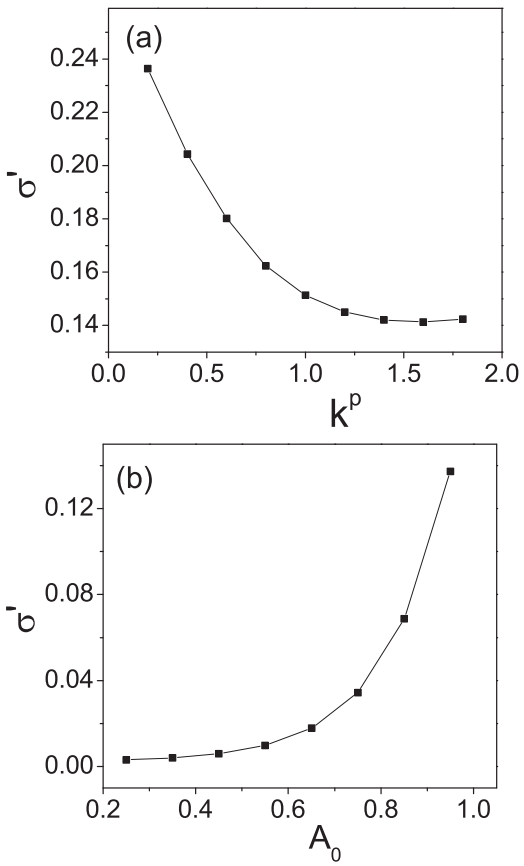

FIG. 4. For the network model described by Eq. (8), the variation of the redefined normalized control error, σ', as functions of (a) the pinning wave number k^p by fixing $A^p = 1$ and (b) the pinning amplitude A^p by fixing $k^p = 0.5$.

Fig. 5. First, it is seen that the modes $A_{1,\ldots,5}$ and A_p are of very different damping rates. More specifically, $A_{2,3}$ are damped to 0 at about $t = 100$, followed by $A_{5,p}$ at about $t = 300$, while $A_{1,4}$ are damped to 0 to about $t = 900$. Clearly, the damping rates of $A_{1,4}$ are much slower than those of $A_{2,\ldots,5}$ and A_p. Second, for the slowly damping modes, $A_{1,4}$, it is observed that from about $t = 500$ they begin to be damping in a "synchronous" fashion, i.e., $A_1(t) \approx A_4(t)$. As during this process we have $A_{2,3,5,p} \sim 0$, and the pair of modes, $A_{1,4}$, thus form a "soliton-like" cluster in the network. The above phenomena are general for the network model and are not affected by the network initial conditions and parameters (e.g., the values of $k_{2,5}$, and the selection of the independent modes).

The fact that $A_{2,3,5,p}$ are damping much faster than $A_{1,4}$ makes it possible to further simplify the model. Let T being the transient period after which $A_{2,3,5,p}$ have been well damped to 0, then for $t > T$ the network dynamics is characterized by only the evolution of $A_{1,4}$, which are governed by the equations

$$dA_1/dt = -\varepsilon_1' A_1 - \varepsilon_1' A^p A_4^* e^{i\Delta\omega t}, \tag{9}$$

$$dA_4/dt = -\varepsilon_4' A_4 - \varepsilon_4' A^p A_1^* e^{i\Delta\omega t}, \tag{10}$$

with $\Delta\omega = \omega_1' + \omega_4'$ the summed frequency of the two hub modes. Differentiating Eq. (9) and using Eq. (10), we can

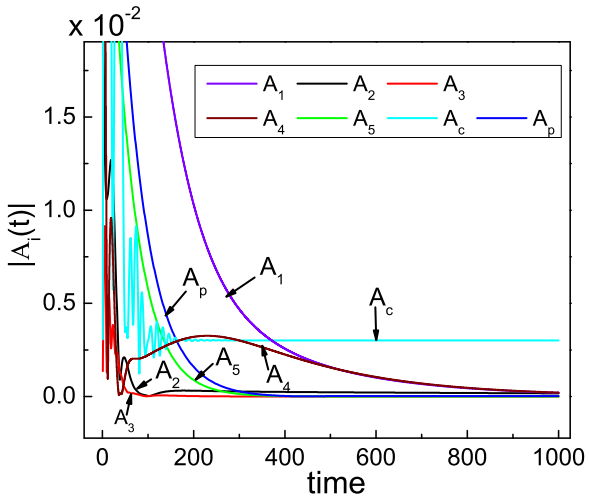

FIG. 5. (Color online) Using the parameters $k_2 = 0.6$, $k_5 = 2.8$, $k_T = 1.25$, $A^p = 1.0$, and $k^p = 0.5$, the time evolution of the mode amplitudes. $A_{2,3}$ are first damped to 0 ($t \sim 100$), followed by $A_{p,5}$ ($t \sim 300$), and, last, $A_{1,4}$ ($t \sim 900$).

obtain the following evolution function for A_1:

$$\frac{d^2A_1}{dt^2} + (\varepsilon_1' + \varepsilon_4' - i\Delta\omega)\frac{dA_1}{dt} + [\varepsilon_1'\varepsilon_4' - \varepsilon_1'\varepsilon_4'(A^p)^2 - i\Delta\omega\varepsilon_1']A_1 = 0. \tag{11}$$

Denoting λ as the damping (growth) rate of A_1, i.e., $A_1(t) \sim \exp(\lambda t)$, in the neighborhood of the target, i.e., when $\sigma \sim 0$, the control performance is characterized by the real part of λ: the smaller Re(λ) is, the faster is the network to be controlled to the target. Inserting the expression of $A_1(t)$ into Eq. (11), we have

$$\lambda^2 + (\varepsilon_1' + \varepsilon_4' - i\Delta\omega)\lambda + \varepsilon_1'\varepsilon_4'[1 - (A^p)^2] - i\varepsilon_1'\Delta\omega = 0, \tag{12}$$

which gives

$$\lambda_\pm = -\Gamma/2 \pm \sqrt{\Gamma^2 - 4[\varepsilon_1'\varepsilon_4' - \varepsilon_1'\varepsilon_4'(A^p)^2 - i\varepsilon_1'\Delta\omega]}, \tag{13}$$

with $\Gamma = \varepsilon_1' + \varepsilon_4' - i\Delta\omega$. The damping rate of A_1 thus is characterized by $\gamma = \text{Re}(\lambda_+)$. [By changing the subscript in Eq. (13), we can also obtain the damping rate for A_4, which slightly differs from γ. This feature is also reflected in Fig. 5, where $A_1 \approx A_4$ for $t > 500$. As such, in the following we will use only γ to characterize the control performance.]

As $\varepsilon' = \varepsilon_0/(1 + k^2)$ and $k_1 + k_4 + k^p = 0$, the damping rate thus can be also expressed as a function of the pinning parameters, i.e., $\gamma = \gamma(\varepsilon_0, k_1, k^p, A^p)$. Using $\varepsilon_0 = 0.15$, $k_1 = 3.8$, and $A^p = 1.0$, we plot in Fig. 6(a) the variation of γ as a function of k^p according to Eq. (13). It is seen that, with the increase of k^p, the value of γ is monotonically decreased. Fixing $k^p = 0.5$, we plot in Fig. 6(b) the variation of γ as a function of A^p, where it is seen that with the increase of A^p, the value of λ is monotonically increased. To compare with the results of numerical simulations (Fig. 2), we present in Fig. 6 also the variation of the control error, γ', as functions of k^p and A^p (in the logarithmic scale), where the theoretical and numerical results are found to be in good agreement.

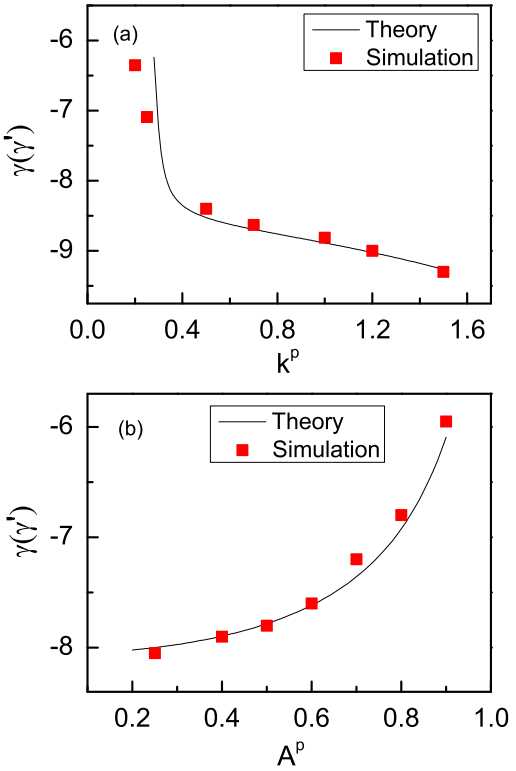

FIG. 6. (Color online) For $\varepsilon = 0.15$ and $k_1 = 3.8$, the damping rate, γ, calculated according to Eq. (13). (a) Fixing $A^p = 1$, the variation of γ as a function of the pinning wave number k^p. (b) Fixing $k^p = 0.5$, the variation of γ as a function of the pinning amplitude A^p. The symbols are the control errors obtained by numerical simulations (Fig. 2) and are presented with the logarithmic scale $\gamma' = 1/\tau \ln \sigma$, with $\tau = 580$ in (a) and $\tau = 617$ in (b).

The performance of distributed pinning can be understood from Eqs. (9) and (10) as follows. The key point lies in the effective coupling strength, $\varepsilon'_{1,4}A^p$, between the two slow-damping modes ϕ_1 and ϕ_4. By increasing A^p, the coupling between the modes will be strengthened, which enlarges the term of mode excitation, $\varepsilon'_{1,4}A^p \exp(i\Delta\omega t)$ and therefore slows down the damping. This property can be also understood from Eq. (13), where we have $\lambda_+ \propto A^p$. The effective coupling strength is also affected by the pinning wave number k^p. Noticing that $\varepsilon'_{1,4} = \varepsilon_0/(1 + k^2_{1,4})$ and $k_{1,4} = -(k_{4,1} + k^p)$ (the resonant condition), the effective coupling strength thus is decreasing with k^p. So by changing the pinning distribution (i.e, the values of k^p and A^p), it essentially adjusts the effective coupling strength between some pairs of resonant modes, which in turn modifies the mode damping rate and affects the control performance.

V. DISCUSSION AND CONCLUSION

The above results of sinusoidal pinning distribution can be generalized to other forms of pinning distributions, as any form of distribution can always be represented by the summation of a series of sinusoidal waves, say, for example, the localized pinning. Localized pinning refers to a situation where the pinning signals are added onto only part of the system sites, which is more practicable and feasible in realistic applications [18,20,29]. To check whether the same phenomena can be observed in localized pinning control, we replace the sinusoidal distribution in Eq. (1) by the following square-wave distribution:

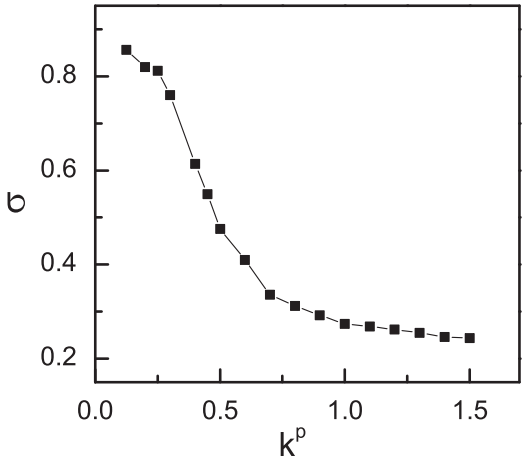

FIG. 7. For the localized pinning distribution described by Eq. (14), the variation of the normalized control error, σ, as a function of the pinning wave number k^p. The other parameters are the same to Fig. 2(b).

$$\varepsilon(x, y) = \varepsilon_0\{1 + \mathrm{sgn}[\sin(k_x x + k_y y)]\}, \tag{14}$$

with sgn(. . .) being the signum function. Thus, the pinning amplitude is alternating between 0 the 2 with a fixed spatial interval characterized by $\boldsymbol{k}^p = (k^p_x, k^p_y)$. Still, we set $k^p_x = k^p_y = k = k^p$. Similarly to the case of sinusoidal distribution, with the increase of k^p the pinning strength tends to the uniform distribution in the space. By the same set of parameters used in Fig. 2, we plot in Fig. 7 the variation of the normalized control error, σ, as a function of the k^p. It is seen that, just like the case of sinusoidal pinning, the control error is monotonically decreased as k^p increases.

Before giving our conclusion, we wish to highlight the significance of complex network models in exploring the turbulent dynamics. While Fourier analysis has been extensively employed in exploring turbulence, to our knowledge, a global picture on the interaction of Fourier modes is still short, especially the connection between the dynamics of the individual modes and the collective behaviors of the whole system. From the viewpoint of complex network, not only the coupling structures of the Fourier modes can be clearly presented but also the roles of each individual mode in affecting the turbulent dynamics can be conveniently figured out, e.g., the importance of each mode can be simply evaluated by its degree or total coupling cost. Having identified the important modes in the network, it would be possible to capture the main features of the system dynamics by a simplified network model which keeps only the important modes. Our studies in the present work shows that, by such a network approach of system simplification, the analysis of the turbulent dynamics indeed could be largely simplified and the mechanisms of distributed pinning becomes straightforward. The same idea of mode identification has been employed in previous studies in controlling spatiotemporal chaos, in

which the important modes are identified by the wavelets transform [13]. Specifically, by modifying a tiny fraction of the wavelet subspaces of the coupling matrix, the stability of the system synchronization can be dramatically enhanced. It is our believing that, with the help of the network science, many new features of turbulent dynamics would be discovered.

In summary, we have studied, both numerically and analytically, the control of 2D drift-wave turbulence by the scheme of distributed pinnings. It is found that, as the pinning distribution tends to nonuniform, the control performance is monotonically deteriorated. Transforming the turbulence equation into the Fourier space, and after a detail analysis on the structure of mode couplings, we have proposed a new model of networked modes, which captures some essential features of the dynamics of pinned turbulence. With the help of this network model, an explicit formula has been obtained on the influence of the pinning distribution on control performance, which are in good agreement with the numerical results. Our studies shed new light on the dynamics of drift-wave turbulence and make a solid step towards the application of pinning control in realistic systems.

ACKNOWLEDGMENTS

This work was supported by the National Natural Science Foundation of China under Grant No. 11375109 and was also supported by the Fundamental Research Funds for the Central Universities under Grant No. GK201303002.

[1] T. Kapitaniak, *Controlling Chaos: Theoretical and Practical Methods in Nonlinear Dynamics* (Academic Press, London, 1996).
[2] H. G. Schuster, *Handbook of Chaos Control* (Wiley-VCH, Weinheim, 1999).
[3] E. Ott, C. Grebogi, and J. A. Yorke, Phys. Rev. Lett. **64**, 1196 (1990).
[4] M. Ding, E. J. Ding, W. L. Ditto, B. Gluckman, V. In, J. H. Peng, M. L. Spano, and W. Yang, Chaos **7**, 644 (1997).
[5] S. Boccaletti, C. Grebogi, Y.-C. Lai, H. Mancini, and D. Daza, Phys. Rep. **329**, 103 (2000).
[6] Y. Kuramoto, *Chemical Oscillations, Waves and Turbulence* (Springer-Verlag, Berlin, 1984).
[7] I. Aranson, H. Levine, and L. Tsimring, Phys. Rev. Lett. **72**, 2561 (1994).
[8] C. Grebogi and Y.-C. Lai, IEEE T. Circuits Syst. (I) **44**, 971 (1997).
[9] M. Jiang, X. Wang, Q. Ouyang, and H. Zhang, Phys. Rev. E **69**, 056202 (2004).
[10] H. Zhang, B. Hu, and G. Hu, Phys. Rev. E **68**, 026134 (2003).
[11] G. Hu and Z. Qu, Phys. Rev. Lett. **72**, 68 (1994).
[12] R. O. Grigoriev, M. C. Cross, and H. G. Schuster, Phys. Rev. Lett. **79**, 2795 (1997).
[13] G. W. Wei, M. Zhan, and C.-H. Lai, Phys. Rev. Lett. **89**, 284103 (2002).
[14] J. Xiao, G. Hu, J. Yang, and J. Gao, Phys. Rev. Lett. **81**, 5552 (1998).
[15] L. Junge and U. Parlitz, Phys. Rev. E **61**, 3736 (2000).
[16] J. Gao, X. Wang, G. Hu, and J. Xiao, Phys. Lett. A **283**, 342 (2001).
[17] G. Hu and K. He, Phys. Rev. Lett. **71**, 3794 (1993).
[18] Z. Cao, P. Li, H. Zhang, F. Xie, and G. Hu, Chaos **17**, 015107 (2007).
[19] S. Guan, Y. C. Zhou, G. W. Wei, and C.-H. Lai, Chaos **13**, 64 (2003).
[20] S. Guan, G. W. Wei, and C.-H. Lai, Phys. Rev. E **69**, 066214 (2004).
[21] G. Tang and G. Hu, Phys. Rev. E **73**, 056307 (2006).
[22] W. Horton, Rev. Mod. Phys. **71**, 735 (1999).
[23] X. Garbet, L. Garzotti, P. Mantica, H. Nordman, M. Valovic, H. Weisen, and C. Angioni, Phys. Rev. Lett. **91**, 035001 (2003).
[24] A. Pironti and M. L. Walker, Control Syst. Mag. **25**, 30 (2005).
[25] T. Pierre, G. Bonhomme, and A. Atipo, Phys. Rev. Lett. **76**, 2290 (1996).
[26] A. K. Sen, Phys. Rev. Lett. **76**, 1252 (1996).
[27] E. Gravier, X. Caron, G. Bonhomme, and T. Pierre, Phys. Plasmas **6**, 1670 (1999).
[28] T. Klinger, C. Schröder, D. Block, F. Greiner, A. Piel, G. Bonhomme, and V. Naulin, Phys. Plasmas **8**, 1961 (2001).
[29] C. Schröder, T. Klinger, D. Block, A. Piel, G. Bonhomme, and V. Naulin, Phys. Rev. Lett. **86**, 5711 (2001).
[30] C. Brandt, O. Grulke, and T. Klinger, Plasma Phys. Controlled Fusion **52**, 055009 (2010).
[31] G. Tang, K. He, and G. Hu, Phys. Rev. E **73**, 056303 (2006).
[32] F. Brochard, G. Bonhomme, E. Gravier, S. Oldenbürger, and M. Philipp, Phys. Plasmas **13**, 052509 (2006).
[33] K. Pyragas, Phys. Lett. A **170**, 421 (1992).
[34] P. Liu, L. Yang, Z. Deng, and X. Wang, Phys. Rev. E **84**, 016207 (2011).
[35] T. H. Stix, Phys. Fluids **12**, 633 (1969).
[36] A. Hasegawa and Y. Kodama, Phys. Rev. Lett. **41**, 1470 (1978).
[37] F. Y. Gang, P. H. Diamond, J. A. Crotinger, and A. E. Koniges, Phys. Fluids B **3**, 955 (1991).
[38] P. H. Diamond, S. I. Itoh, K. Itoh, and T. S. Hahm, Plasma Phys. Control. Fusion **47**, R35 (2005).
[39] A. Hasegawa and K. Mima, Phys. Rev. Lett. **39**, 205 (1977).
[40] M. J. Burin, G. R. Tynan, G. Y. Antar, N. A. Crocker, and C. Holland, Phys. Plasmas **12**, 052320 (2005).
[41] S. Y. Yang, Y. C. Zhou, and G. W. Wei, Comput. Phys. Commun. **143**, 113 (2002).
[42] R. Albert and A.-L. Barabási, Rev. Mod. Phys. **74**, 47 (2002).
[43] X. F. Wang and G. Chen, Physica A **310**, 521 (2002).
[44] J. Zhao, J. Lu, and Q. Zhang, IEEE T. Circuits Syst. **56**, 514 (2009).
[45] L. Yang, X. G. Wang, Y. Li, and Z. Sheng, Europhys. Lett. **92**, 48002 (2010).
[46] T. Nishikawa, A. E. Motter, Y.-C. Lai, and F. C. Hoppensteadt, Phys. Rev. Lett. **91**, 014101 (2003).
[47] X. G. Wang, Y.-C. Lai, and C. H. Lai, Phys. Rev. E **75**, 056205 (2007).